Swiss J Geosci (2017) 110:613–630
DOI 10.1007/s00015-017-0261-8

Three-dimensional modelling of folds, thrusts, and strike-slip faults in the area of Val de Ruz (Jura Mountains, Switzerland)

Davood M. Yosefnejad[1] · Thorsten J. Nagel[2] · Nikolaus Froitzheim[1]

Received: 15 February 2016 / Accepted: 13 January 2017 / Published online: 2 March 2017

Abstract The Val-de-Ruz syncline is a northeast-southwest trending, rhomb-shaped synclinal basin in the internal part of the central Jura Mountains. The Mesozoic sediment succession is decoupled from the basement by a décollement horizon in Middle Triassic evaporite-bearing layers at depth and folding is associated with southeast-dipping thrust splays rooting into this décollement. The folds and thrusts also interfere with a system of N-S striking, sinistral strike-slip faults. A 3D model was constructed from the following input data: A digital elevation model, the 1:25,000 geological map of Switzerland, published contours of the top of basement based on drilling and seismics, and nine newly constructed cross-sections. The latter are based on surface geology and published seismic data. Cross-sections parallel to the northwestward transport direction, i.e. perpendicular to the overall strike, are line balanced. Anticlines are interpreted as faulted detachment folds, which initiated by buckling and associated flow of evaporites from synclinal to anticlinal areas. Anticlines were later broken by northwest-vergent thrusts and subsequently developed into fault-propagation folds during décollement from the basement and northwestward translation. The model assumes no faulting in the pre-Mesozoic basement and no hidden flat-ramp tectonics in the subsurface in order to account for structurally high positions. As a consequence, the modelled cumulative, post-deformation thickness of Triassic strata locally exceeds 1500 m, which we find in accordance with regional observations. From the geological 3D model, new cross-sections in any desired orientation and tectonic thickness variations of the layers can be extracted. The three output cross-sections presented are in excellent agreement with published reflection seismic data. The most important features of our model are (1) large thickness variations due to lateral flow of evaporites, and (2) new and plausible explanation of structural highs in terms of accumulation of Triassic strata by lateral flow.

Keywords 3D modelling · Jura Mountains · Val de Ruz · Detachment fold

1 Introduction

The Jura Mountains in western Switzerland are a foreland fold-and-thrust belt and represent the youngest, most external part on the northwestern side of the Alpine orogen (Fig. 1; Laubscher 1961, 1965; Burkhard 1990; Philippe et al. 1996; Sommaruga 1999). They describe the shape of a northwest-facing crescent, which at its southern end merges with the most external chains of the Western Alps. To the northeast of this junction, the Swiss Molasse Basin, representing the Oligocene to Miocene foreland basin of the Alps, lies between the Jura Mountains and the Alps. The mountain range itself consists of Mesozoic to Tertiary sedimentary rocks with upper Jurassic platform carbonates (Malm) forming the backbones of prominent anticlines. To

Editorial handling: S. Schmid.

Electronic supplementary material The online version of this article (doi:10.1007/s00015-017-0261-8) contains supplementary material, which is available to authorized users.

✉ Davood M. Yosefnejad
davood.yosefnejad@uni-bonn.de

[1] Steinmann-Institut, University of Bonn, Poppelsdorfer Schloss, 53115 Bonn, Germany

[2] Department of Geoscience, Aarhus University, Høegh-Guldbergs Gade 2, 8000 Aarhus, Denmark

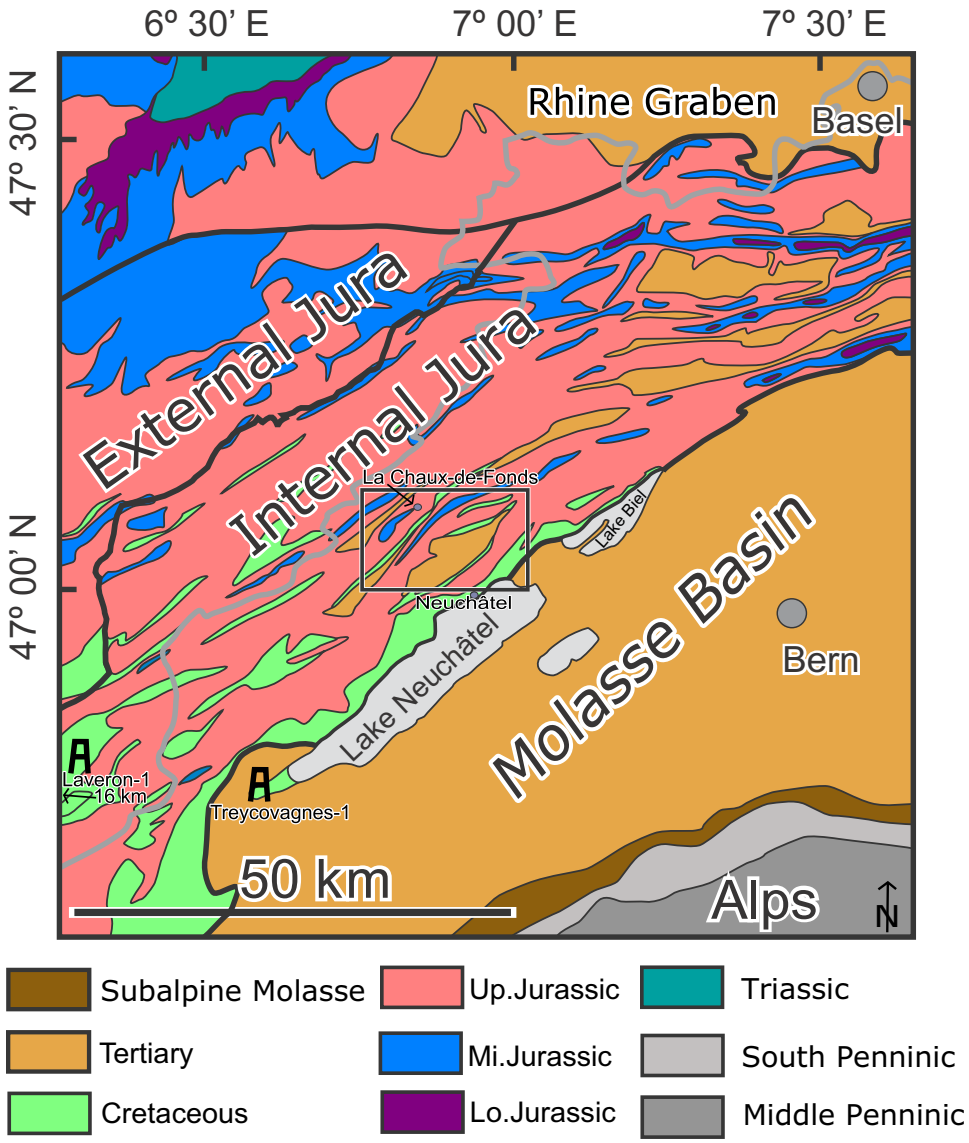

Fig. 1 Geological overview map of the central Jura Mountains based on the Geological Map of Switzerland (Bundesamt für Wasser und Geologie 2005). *Thick black lines* are the front of the Jura in the North, the boundary between Internal and External Jura in the middle, and the Jura/Molasse boundary in the South. *Grey line* is the French/Swiss border. Locations of drill holes Laveron-1 and Treycovagnes-1 are indicated. *Rectangle marks* the map area of Fig. 2

the West, the sediment succession of the Jura Mountains is thrust over the fill of the Rhone-Bresse Graben by several kilometres. In the eastern Jura Mountains, shortening of the sedimentary succession ceases gradually and the last remaining anticlines in the Mesozoic series plunge under the sediments of the Molasse Basin. The internal, topographically higher part of the Jura Mountains is characterized by faulted detachment folds ("Folded Jura" or "Haute Chaîne"), whereas the external part ("Plateau Jura") displays lozenge-shaped, undeformed plateaus ("Plateaux") separated by faulted anticlines ("Faisceaux"). Deformation started in Middle Miocene and lasted at least into Pliocene times (Kälin 1997), with some evidence for still on going folding in the most external part of the Jura (Madritsch et al. 2010). The folded Jura is classic for studying thin-skinned tectonics and several pioneering studies on décollement tectonics and cross-section balancing were performed in this mountain chain (Buxtorf 1916; Laubscher 1961, 1965; Mitra 2003; Affolter and Gratier 2004).

The tectonic evolution of the Jura Mountains was governed by decoupling along evaporites in the Middle Triassic (Muschelkalk) and Upper Triassic (Keuper) sedimentary successions. Isopachs of the Muschelkalk and Keuper are similar in shape to the outline of the Jura Mountains, together reaching 1000 m and more in the internal western part while they are only several tens of meters thick in the adjacent Helvetic units in the Alps (Loup 1992; Sommaruga 1997, 1999; Affolter and Gratier 2004). This suggests that the lateral termination of the Jura Mountains to the East and to the South results from the pinching-out of the evaporites. The fact that the Mesozoic strata are spectacularly folded in the Jura Mountains whereas folding is hardly visible in the Molasse Basin has led some researchers to seek the origin of

the folding in deformation of the basement under the Jura (e.g. Aubert 1945; Pavoni 1961; Ziegler 1982). Others have assumed that shortening in the Jura Mountains is completely allochthonous and that the corresponding shortening of the basement took place on the other side of the Molasse Basin within the Alps, hence, tens of kilometres to the Southeast (Buxtorf 1907, 1916; Laubscher 1961). This theory, called the "Fernschubhypothese", is now accepted by most authors although it is acknowledged that pre-existing Paleozoic and Tertiary normal faults played a role in the localization and development of contractional structures, i.e. folds and thrusts (Ustaszewski and Schmid 2006; Malz et al. 2016). The generally southeastward- or hinterland-dipping thrusts in the Jura Mountains are assumed to root into a major floor thrust located within or at the bottom of the Triassic formations (Buxtorf 1907, 1916; Burkhard 1990). The mechanical basement beneath this floor thrust includes Variscan basement and locally also Permo-Carboniferous troughs (Diebold 1988; Madritsch et al. 2008) as well as Lower Triassic fluvial sediments (Buntsandstein). The floor thrust continues beneath the Molasse Basin and connects shortening of the Mesozoic-Tertiary cover in the Jura mountains with basement shortening in the external zone of the Alps (e.g. Laubscher 1961). Its existence is confirmed by highly deformed Triassic rocks found in wells in the Molasse Basin in the hinterland of the western (Fischer and Luterbacher 1963) and eastern Jura Mountains (Jordan 1992). The relatively weak deformation in the post-Triassic rocks in the subsurface of the Molasse Basin is explained by the thickness of the Tertiary Molasse sediments, which prevented the Mesozoic layers to lift off and form anticlines or thrust duplexes (e.g. Laubscher 1961). In the ductile Triassic sediments, however, folds with wavelengths around 10 km and a few hundred meters amplitude exist beneath the Molasse Basin as well (Bitterli 1972; Sommaruga 1995). Towards northwest the thickness of the Molasse sedimentary pile progressively decreases while the thickness of the soft Triassic succession increases, allowing the post-Triassic succession to detach from the basement and to become folded and imbricated in the Jura Mountains.

Compared to the Swiss Molasse Basin, which was subject to hydrocarbon prospection, the density of wells and reflection seismic lines is scarce in most of the Jura Mountains and the subsurface architecture remains a matter of debate. In particular, the existence of structurally high domains, i.e. areas where the entire Mesozoic succession is at a relatively high elevation, has been interpreted in controversial ways. These high domains have been explained by (1) local basement highs (Guellec et al. 1990; Pfiffner et al. 1997) or (2) exceptional thickness of Triassic strata, either of sedimentary or tectonic origin (e.g., Sommaruga 1997; Affolter and Gratier 2004). Recently, Schori et al. (2015) have proposed (3) regional doubling of the lower part of the sedimentary succession above the mechanical basement for the Chasseral area northwest of Lake Biel. This doubling would be the result of a large-offset splay rooting in the floor thrust and forming a map-scale upper flat in Middle Jurassic (Dogger) claystone (Opalinus clay). It would thus account for about 800 m of structural uplift.

Here we present a three-dimensional digital model of the architecture of the 1:25,000 geological map sheet "Val de Ruz" (Bourquin et al. 1968), which is located northwest of the northern end of Lake Neuchatel in the central Jura Mountains (Figs. 1, 2). The area contains the wide Val-de-Ruz syncline and a series of thrust-related anti- and synclines to the northwest and to the southeast. It is perfectly suitable for building a three-dimensional digital model and testing it since an excellent geological sheet is available, abundant published and interpreted reflection seismic data exist. Moreover, the overall structural architecture including the top of the mechanical basement has been the subject of extensive investigation (Sommaruga 1997, and references therein). The model was built using the structural modelling software package Move (Version 2014) of Midland Valley Corporation. Three-dimensional geometric modelling has successfully been used to explore complex tectonic structures (Tanner et al. 2003; Maxelon and Mancktelow 2005; Marquer et al. 2006; Zanchi et al. 2009; Sala et al. 2014). Apart from visualization, a major advantage is that the process of modelling implies testing the input data for consistency and testing tectonic hypotheses for their geometric feasibility. Moreover, modelling software allows the extraction of additional information from the model, e.g. cross-sections in any desired orientation, orientation statistics, and volumes or thicknesses of geological bodies. On the other hand, geological data generally need to be simplified for the modelling process, which may lead to mistakes. Moreover, it has to be kept in mind that a geometrically feasible model is not necessarily correct. In the present study, we constructed a model of the Val de Ruz fold structures (1) in order to investigate if simple geometric assumptions (see below) lead to an acceptable 3D-architecture, and (2) which deformation style would be suggested by the derived architecture.

Our contribution strongly builds on the work of Sommaruga (1995, 1997, 1999) and Sommaruga and Burkhard (1997), who interpreted industrial seismic profiles from the southern Jura Mountains and the Molasse Basin and combined them with the surface geology into a coherent tectonic picture of the Internal Jura Mountains around the Val de Ruz and the adjacent Molasse Basin. We took the results of these studies as input for our modelling as our newly constructed cross-sections largely agree with their approach regarding structural style. Like these authors, we assume no deformation in the basement and a simple ramp-

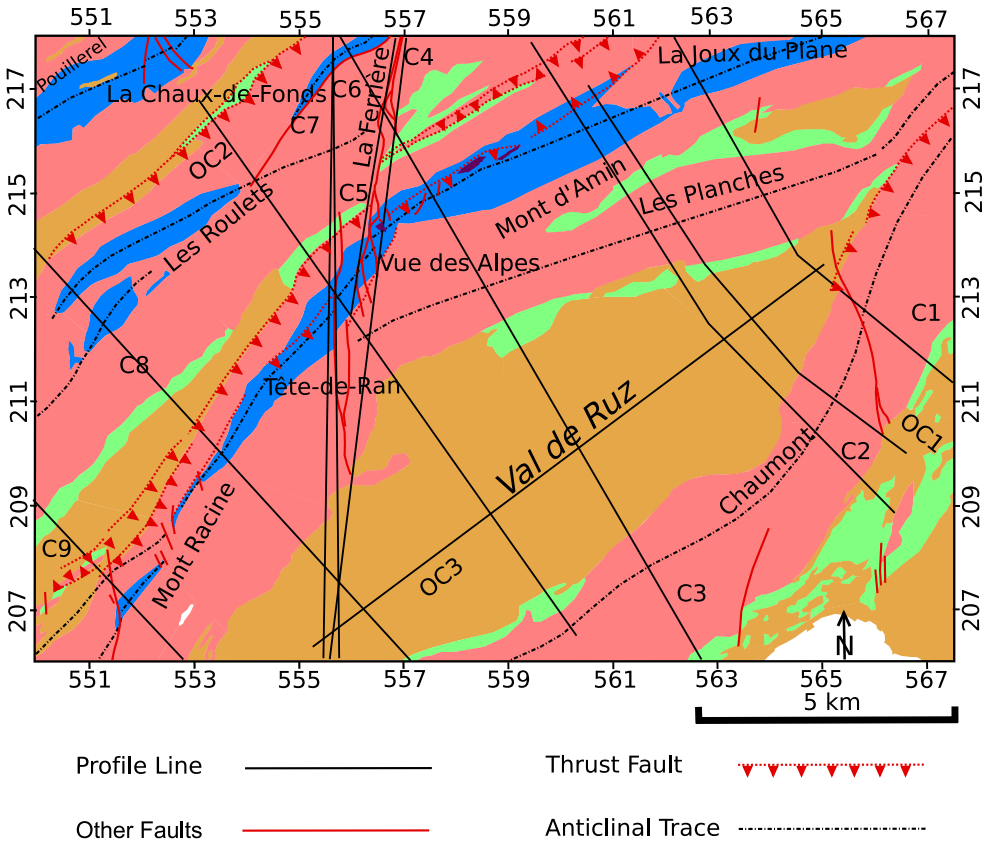

Fig. 2 Simplified geological map of Val de Ruz without Quaternary cover, based on Atlas géologique de la Suisse 1:25,000, feuille 51 Val de Ruz (Bourquin et al. 1968). Profile lines of input profiles (C1–C9) and output profiles (OC1 to OC3) are indicated. Coordinates refer to the kilometric grid of Switzerland. For the *colours*, see Fig. 3

flat architecture, in which thrusts observed at the surface diverge as splays from the floor thrust at the top of the mechanical basement. We actually imply rather free formation of anti- and synclines in the Triassic rocks and comparably small-offset thrusts in the sedimentary pile above. This simple approach leads to extremely well balanced cross-sections. The model predicts originally thick Triassic sequences, which are considerably over-thickened below antiforms. Accordingly, bulk shortening is limited, i.e. around 7% and at most 17%. We will discuss the proposed architecture, the inherent assumptions and alternative views in the light of regional observations in detail after the presentation of the model.

2 Structural edifice in the study area

The study area is characterized by faulted anticlines, which expose Dogger and Malm in their cores, forming topographic highs and synclines, which contain Lower Cretaceous and thin Tertiary sediments (Fig. 2). The anticlines trend overall southwest-northeast. They are dominantly thrust towards northwest over the synclines but some backthrusting occurs as well. In the southeast of the study area, the large Chaumont Anticline exposes formations of the Malm. North of Lake Neuchatel, the trend of this anticline changes from north-northeast in the north to northeast further south. An associated thrust cutting across the external limb is only exposed in the Northeast. Towards southwest, this thrust disappears below the Quaternary cover of the Val de Ruz. An additional very minor anticline appears more internally just north of Lake Neuchatel, exposing a narrow stripe of Malm in the core.

Northwest of the Chaumont Anticline follows the rhomb-shaped Val-de-Ruz syncline. It contains Oligo-Miocene Molasse sediments but is mostly covered by fluvio-glacial Quaternary sediments. Where not covered by the Quaternary, the dip of the Mesozoic and Tertiary strata is mostly 0°–20° towards southeast. Also the smooth, gently northwestward rising topography suggests a rather consistent dip. The dip of sedimentary strata is in good agreement, i.e. in parallelism with the top of the mechanical basement, which was contoured using regional reflection seismic data and is interpreted as the base of the Muschelkalk strata (Sommaruga 1997). The local reflection seismic data across the Val de Ruz is generally of very good quality and shows a simple, undeformed pile of reflectors parallel to the contoured top-basement surface (Sommaruga 1997, 1999). Hence, the Val de Ruz appears to expose an internally almost undeformed, complete sedimentary pile on top of a hangingwall thrust flat. The syncline might thus provide a reference section to estimate the original thickness of the

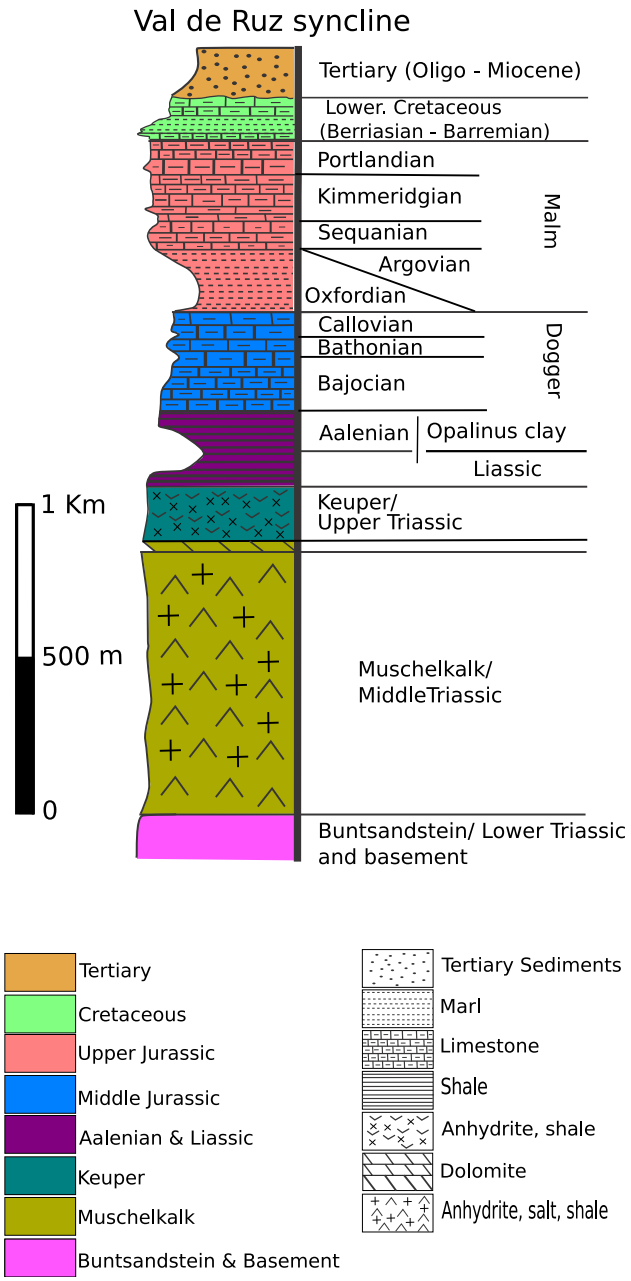

Fig. 3 Stratigraphic column of Val de Ruz syncline, simplified from Sommaruga (1997). These *colours* are used in Figs 2, 4, 5, 7 and Appendix 1

sedimentary pile (Sommaruga 1999). This parameter is essential for the construction of line-balanced cross-sections as such sections typically assume constant layer thicknesses.

To the northwest of the Val-de-Ruz syncline follows the dominating anticline on the map sheet, which widely exposes Middle Jurassic strata in its core. The southwestern part of this anticline (Mont Racine, Tête de Ran) trends northeast to north-northeast, the northeastern part (Mont d'Amin, Joux du Plane) trends east-northeast. In the area where the trend changes, the anticline is offset by a system of minor, en-échelon strike-slip faults, which form the southern tip of the major sinistral La Ferrière strike-slip fault (Tschanz 1990; Sommaruga 1997). These strike-slip faults are located between the profile traces C4 and C7 shown in Fig. 2. Similarly oriented, small strike-slip faults occur also in other parts of the area, e.g. at Chaumont and Mont Racine. The Mont d'Amin—La Joux du Plane anticline on the eastern side of the strike-slip zone is not directly adjacent to the Val de Ruz syncline. A tight syncline with Cretaceous in the core and a gentle anticline (Les Planches Anticline) exposing Malm appear in between. Hence, anti- and synclines are discontinuous across the strike-slip fault system and not only rigidly displaced, suggesting that the faults were active as tear faults during folding and thrusting. In the northwestern corner of the map sheet, there is another couple of complex anticlines (Les Roulets and Pouillerel) separated by synclines. The structurally deepest syncline is that of La Chaux-de-Fonds containing Tertiary beds up to Late Middle Miocene age. The geometries of these folds outside the map sheet to the north are actually substantially different to both sides of the La Ferrière fault (Sommaruga 1997). The particular shape of the Val-de-Ruz syncline results from the southwestward divergence of the Les Planches anticline and the Chaumont anticline and the following convergence outside the study area to the southwest (Figs. 1, 2). Such truly 3-dimensional structures are seen at several places in the Jura Mountains, exposing further rhomb-shaped synclines such as the Delémont syncline (Keller and Liniger 1930). This architecture may partly result from simultaneous distributed buckling and subsequent lateral growth of anticlines into a non-cylindrical pattern (Grasemann and Schmalholz 2012). On the other hand, pre-existing faults inherited from Rhine Graben rifting also play an important role (Laubscher 1972).

The exposed Mesozoic-Tertiary succession is an alternation of competent limestone and incompetent marl and shale layers (Fig. 3; Bourquin et al. 1968; Sommaruga 1997, 1999). Thin Tertiary sediments of the Molasse rest unconformably on the Lower Cretaceous strata consisting of alternating marls and limestones. The underlying Middle and Upper Malm formations are formed by massive limestones, which represent the major competent unit and define local fold geometry and topography. The lithologies of the Lower Malm are thick marls ("Argovian"). Below a brief sedimentary gap follow dominantly thick, oolitic limestones with some intercalations of marls in the Dogger strata. Lower Dogger (Aalenien) and the uppermost Liassic are represented by a prominent black shale, the Opalinus clay (Fig. 3). The latter is the lowermost unit in the study area, which is exposed in structural continuity. It occurs only in small outcrops in the core of the Mont d'Amin anticline and also, together with some slivers of Liassic

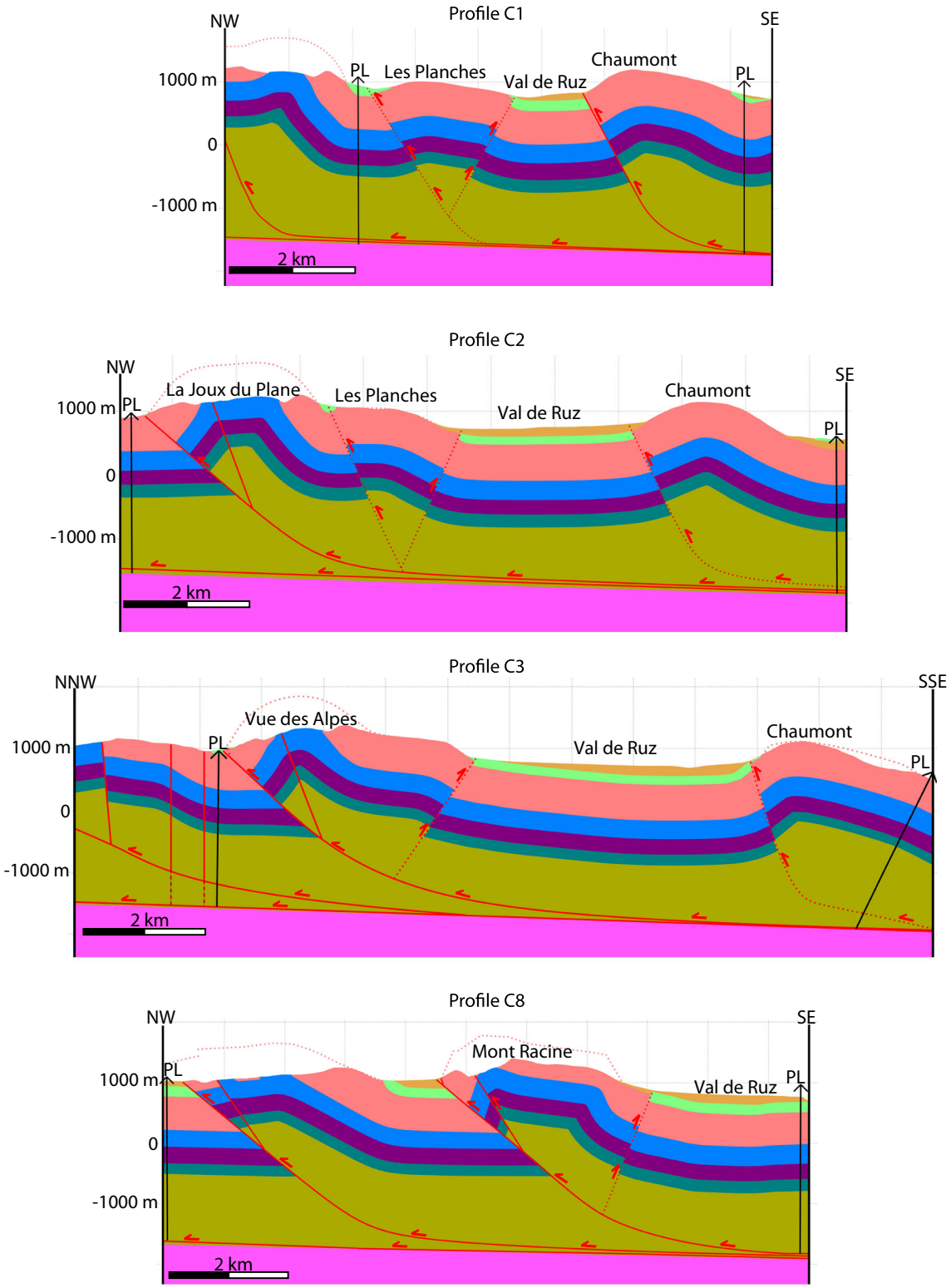

Fig. 4 Input profiles. Location of the profiles: see Fig. 2. PL: Pin lines for line balancing. Thrusts exposed at the surface are shown as *solid red lines*, blind thrusts are *dashed*. Tear faults are subvertical and *dashed* in the lower part since their extension is uncertain. *Colours* see Fig. 3

rocks, along the La Ferrière fault. The deeper units do not reach the surface. Their thickness and the thickness of the Opalinus clay in the study area are only inferred from seismic interpretation and correlation with well logs outside the study area (Sommaruga 1997). Sommaruga (1997, 1999) distinguishes a Triassic Unit I (corresponding

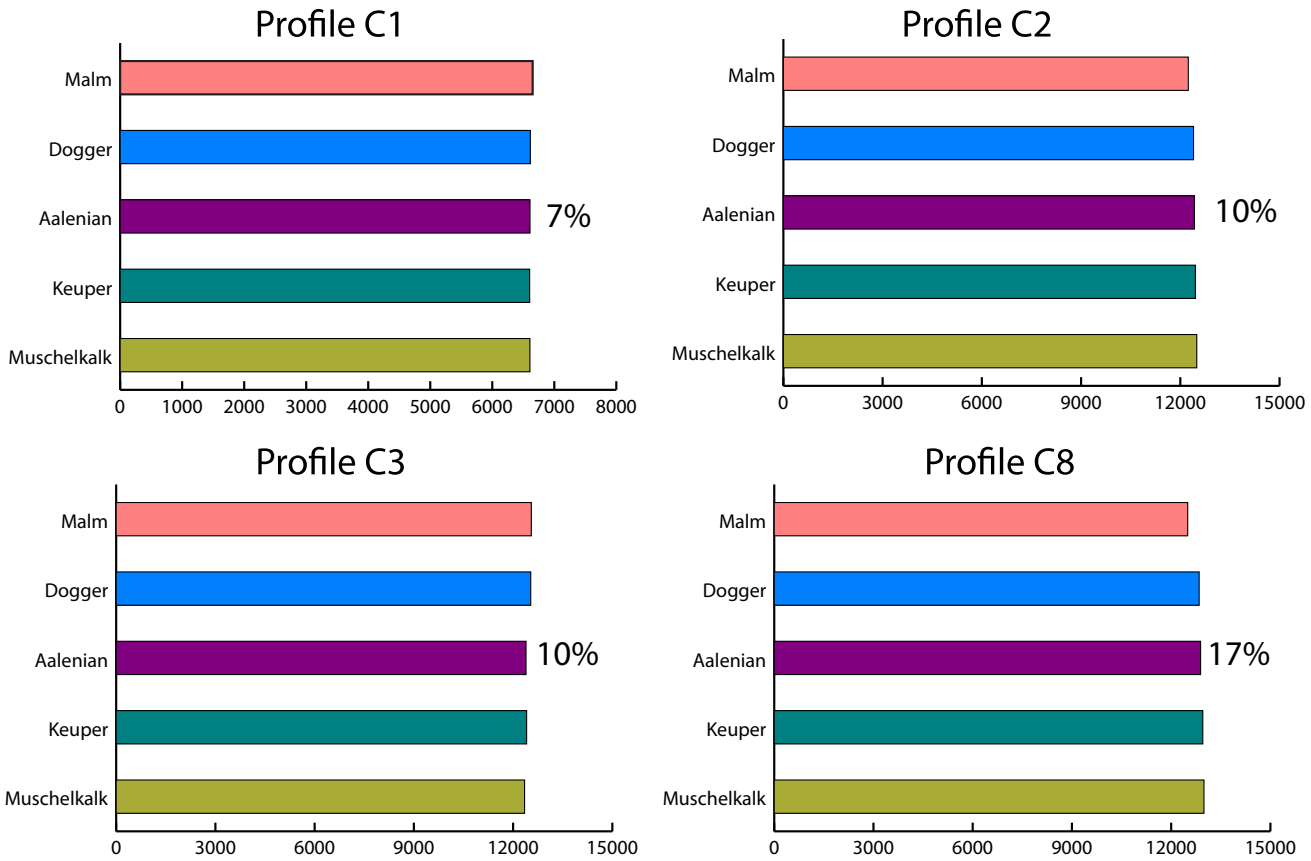

Fig. 5 Line balancing for the input profiles in Fig. 4. The *bars* show the length of the top of the respective stratigraphic units, e.g. "Malm" means the length of the top of the Malm. *Numbers on the horizontal axis* are meters. Average percentage of shortening of the layers is indicated for each profile. All profiles are well balanced, i.e. differences in bed length are small

to Keuper in the Germanic facies) and a Triassic Unit II (corresponding to Muschelkalk). Both units are extremely ductile and can contain significant portions of evaporites (rock salt and/or gypsum) besides dominantly shallow marine limestones in the Muschelkalk and terrestrial clastic sediments in the Keuper series. Sommaruga (1997) interprets a distinct reflector (reflector H) within the Triassic series as dolomites typically found in the uppermost Muschelkalk. Because of the indirect evidence, however, she uses the terms Triassic Unit 1 and 2. We adopt the thickness of Triassic series I and II from her correlation but for simplicity use the terms Muschelkalk and Keuper, respectively. The main décollement horizon/floor thrust in this part of the Jura Mountains is assumed to be at the base or within the Muschelkalk strata, although few well data in the wider vicinity suggest considerable deformation and internal stacking also in the Keuper formations (Sommaruga et al. 2012). The view that there is little thrusting within the Keuper in the study area, is supported by the identification of the above mentioned reflector H. This reflector appears consistently deformed with the younger strata and involved in the ramp-flat architecture. Units below the floor thrust are Lower Triassic fluvial sandstones (Buntsandstein), possible Permo-Carboniferous graben fill, and Variscan basement, lumped here together as mechanical basement. Surfaces below reflector H, in particular the very important top of the mechanical basement, are not very clearly resolved in seismic sections; hence some uncertainty remains about its actual depth.

3 Three-dimensional model

3.1 Data and building strategy

We constructed nine cross-sections as input constraints for the 3D-model (Figs. 2, 4) (to see all nine cross-sections, see Appendix 1 or 3D file in the electronic supplementary material). Four of these are in the vicinity of the La-Ferrière fault and oriented north south, parallel to the fault, in order to define the geometry in this structurally complicated zone. The other cross-sections are oriented perpendicular to the local strike of bedding and fold axial planes, i.e. broadly northwest-southeast (Fig. 2). Using geological

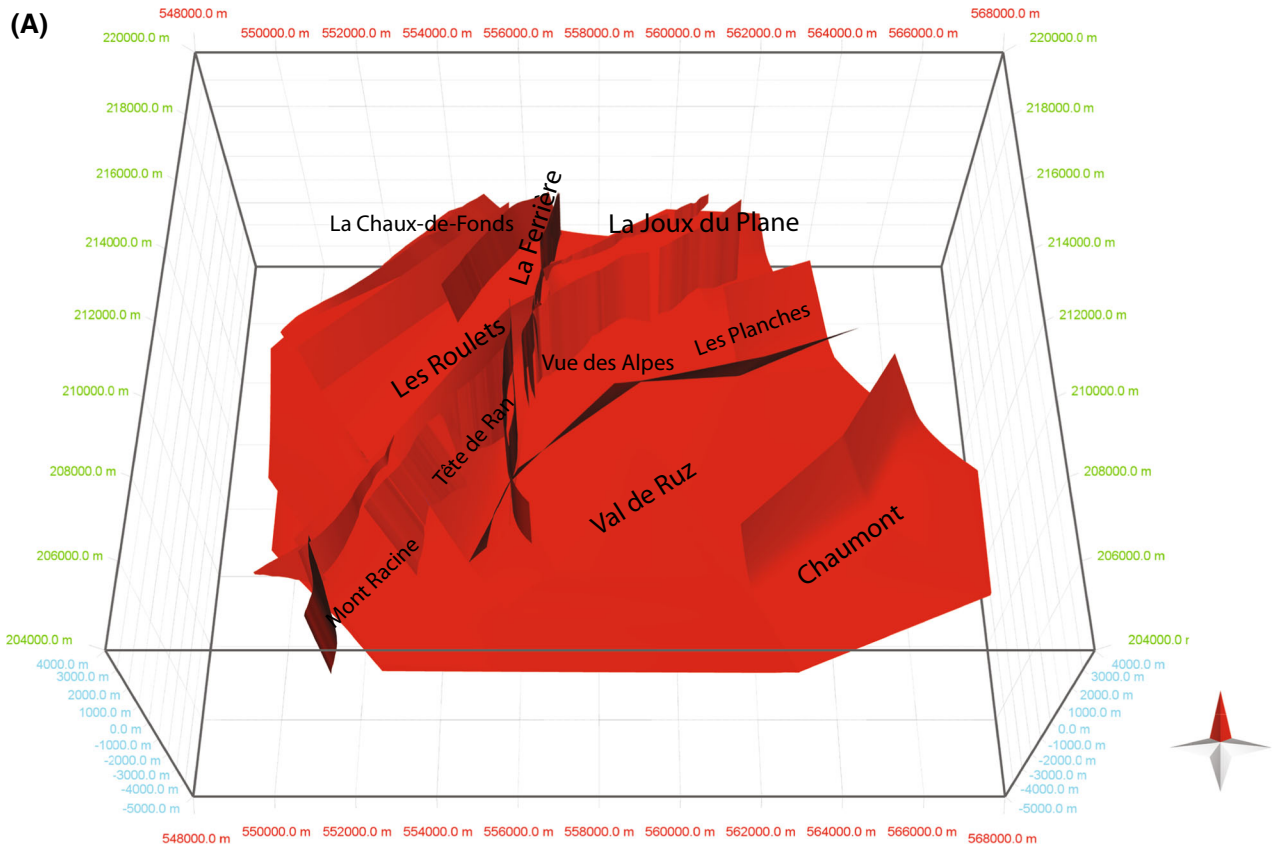
(A)
La Chaux-de-Fonds
La Ferrière
La Joux du Plane
Les Roulets
Vue des Alpes
Les Planches
Tête de Ran
Val de Ruz
Chaumont
Mont Racine

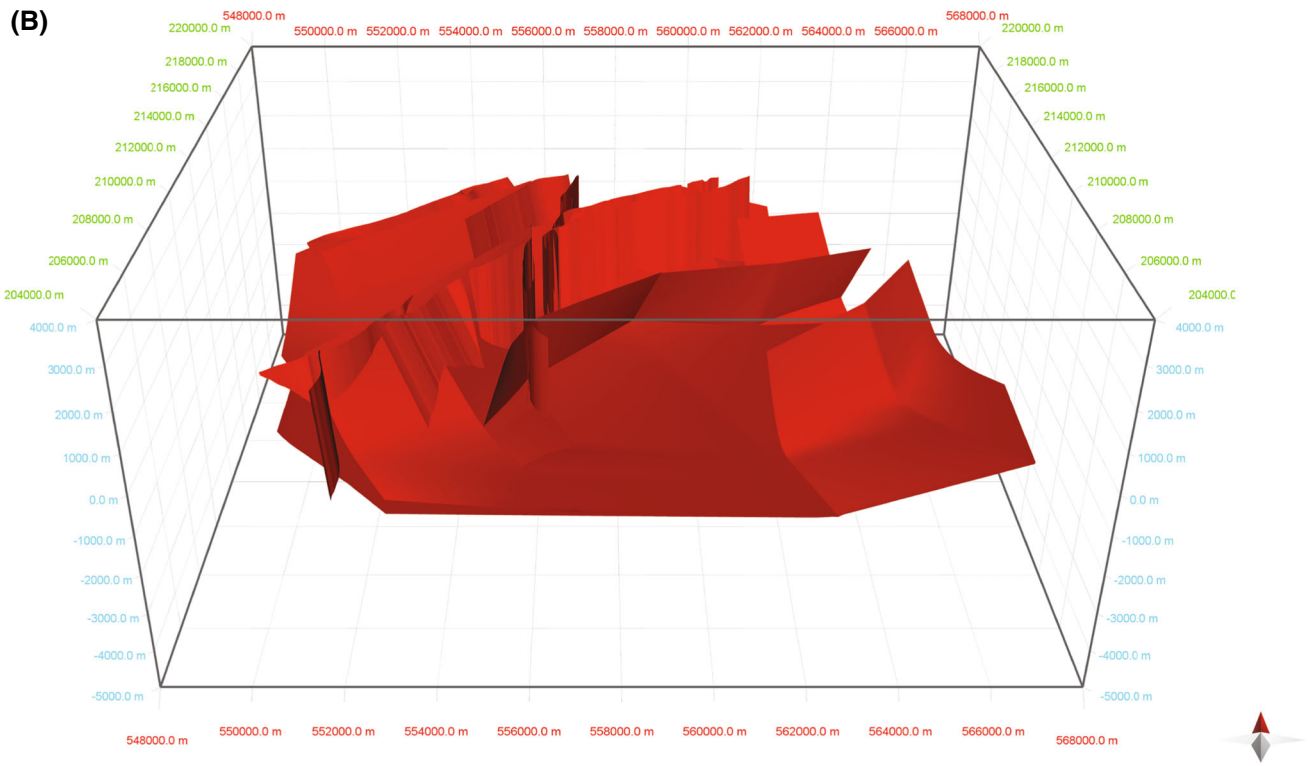
(B)

◀**Fig. 6** Fault surfaces of the model, viewed in two different directions. North–south oriented faults are parts of the La Ferrière strike-slip fault system. North direction indicated by *red* peak of the compass rose. *Green* and *red numbers around the box* are Swiss coordinates, *blue numbers* depth

surface information (Bourquin et al. 1968) and assuming a floor thrust at the top of the contoured mechanical basement at the base of the Muschelkalk series (Sommaruga 1999), the construction follows concepts of ramp-flat thrusting and associated fault-bend folding (e.g. Suppe 1983; Suppe and Medwedeff 1990). We used classic "thrust-belt rules" allowing e.g. to predict the ramp dip from back limb orientation or to infer the lower end of a ramp using the axial plane of the syncline at the bottom of the back limb (Suppe 1983). The lithological column is somewhat simplified (Fig. 3). However, as we assume coherent deformation from the Tertiary down to the top of the Muschelkalk series, lithological boundaries in Fig. 4 are merely passive markers. The thickness of the strata from the Cretaceous series down to the Keuper series were taken from the depth conversion of Sommaruga and Burkhard (Sommaruga and Burkhard 1997; their Fig. 7.1–4), which for the exposed units in the study area are very similar to thicknesses estimated in the field (Guellec et al. 1990). Parallel folding with constant layer thickness was assumed for the construction. The location of the floor thrust was taken from Fig. 20 of Sommaruga (1999), a regional contour map based on depth conversion of seismic sections and drill-hole data. According to this map, the top of the mechanical basement dips shallowly southward in the model area, ranging from ca. 1600 m below sea level in the North to ca. 1900 m below sea level in the South. However, as mentioned above, this surface is rather poorly imaged on the seismic lines. A caveat about the accuracy of this contour map in the study area is posed by the fact that the only nearby well that reaches the Lower Triassic sandstones, the well "Treycovagnes-1" (Fig. 1; Sommaruga et al. 2012), enters the Lower Triassic ca. 300 m higher than the general trend of the contour lines would predict, which causes the proposition of a local basement high in the map of Sommaruga (1999). The well is located outside the map sheet southwest of Lake Neuchatel at the boundary between Molasse and folded Jura (Fig. 1), but it is the only well in a wider area that penetrates the Muschelkalk series. Also well "Laveron-1" located some 50 kilometres west of Lake Neuchatel in the Plateau Jura corresponds to a local basement high in the contour map (Sommaruga 1999). Hence, the actual depth of the mechanical basement may be somewhat shallower, and consequently also the thickness of the Muschelkalk series smaller than in the profile constructions (Fig. 4). Seismic lines and interpreted geological cross-sections presented in Sommaruga (1997) were considered in our construction. Our sections are quite similar to Sommaruga's and the ones presented recently in a report on the geothermal potential of the area (Groupe de travail PGN 2008).

During profile construction we assume that the south-east-dipping fore-thrusts continue through the Muschelkalk series and curve into parallelism with the top of the mechanical basement, but they might as well root within the Muschelkalk series or even dissipate in distributed deformation. The northwest-dipping back-thrusts are interpreted to terminate when reaching more prominent fore-thrusts. The NW–SE-oriented profiles C1, C2, C3 and C8 were checked for plausibility by line balancing between pin lines placed in the synclines. The line length is well balanced for all cross-sections (Fig. 5). The thickness of the Muschelkalk in the profiles is variable; it results from the distance between the base of Keuper and the top of the basement. We allow distributed deformation (flow) in this unit at locations where flow explains observations at the surface better than a pure ramp-flat geometry. For example, the saucer shape of some synclines (e.g. Profile C1), with a variable thickness of the Muschelkalk under the syncline, is a feature that would not occur if the folds were pure fault-bend or fault-propagation folds; if they were, synclines would be defined as lower flats and the bedding would remain perfectly parallel to the dip of the floor thrust in south-eastward direction until being cut off by the next, structurally higher thrust below the adjacent anticline (Suppe 1983; Suppe and Medwedeff 1990). However, in several places in the Jura Mountains, the domains immediately below thrusts appear to be structurally lifted, suggesting a continuation of the forelimb of the antiform below the thrust. A prominent example is the Weissenstein anticline in the northern Jura Mountains, where this observation has led to the rather far-fetched proposition of a series of small blind backthrusts beneath the ramp (Laubscher 2003). The saucer shape of synclines illustrates that the folds originally formed as detachment folds. Buckling of the higher Mesozoic succession under horizontal compression was accommodated by lateral flow of Muschelkalk evaporites from synclinal to anticlinal areas, leading to the observed thickness changes under the synclines even before thrusting started (Sommaruga 1999; Mitra 2003). Folds subsequently developed into fault-propagation folds and where then broken and imbricated by the northwest-directed thrusts. This scheme is also supported by the fact that in the entire Jura Mountains, cross-sections constructed in a pure ramp-flat approach, i.e. using constant thickness also in the Triassic strata, systematically run into balancing problems, if the applied sediment thicknesses are derived from the lower flats in the synclines (see above). Since the assumed thickness of the

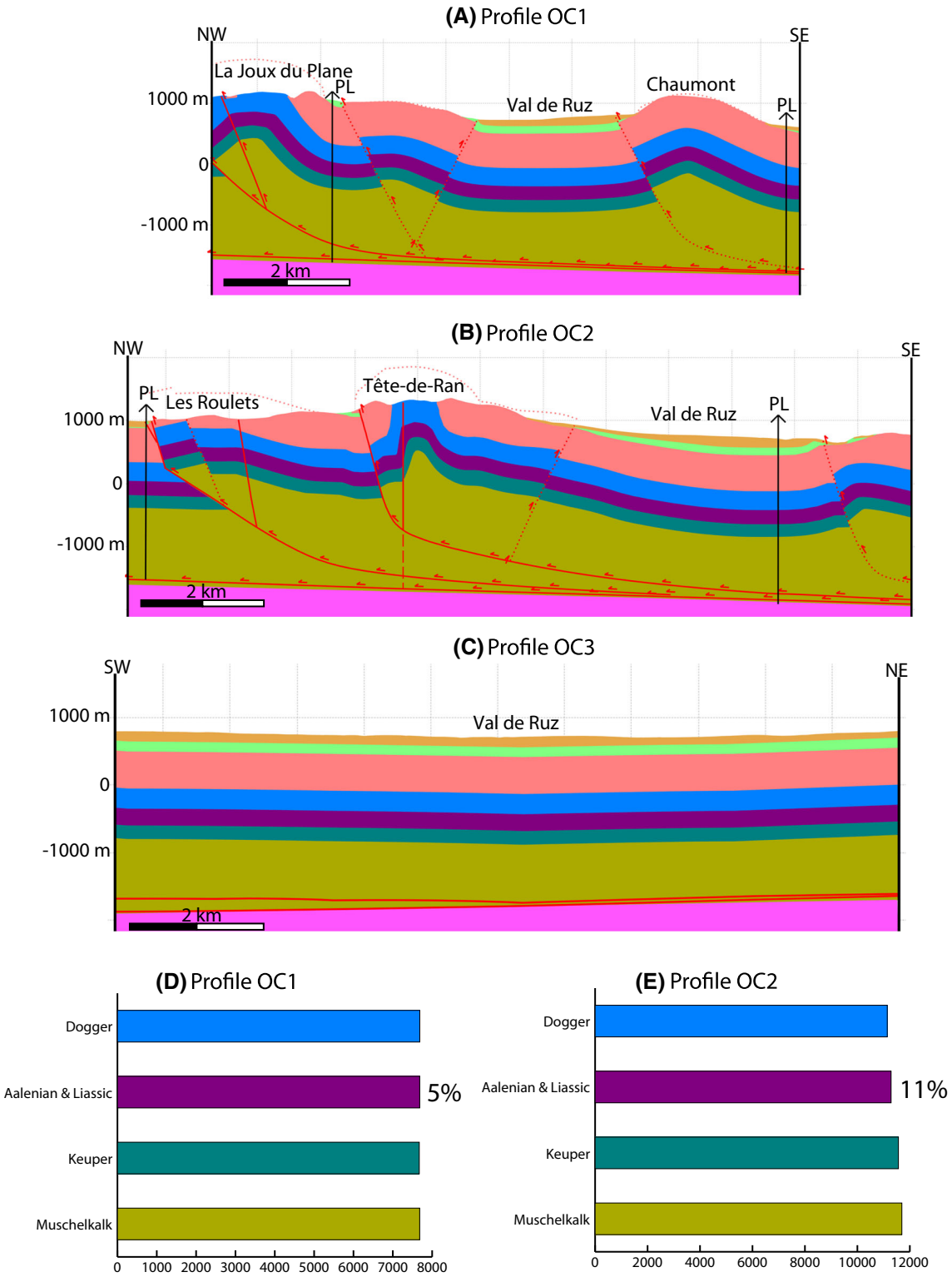

Fig. 7 **a**–**c** Profiles extracted from the model. Location of the profiles: see Fig. 2. PL: Pin lines for length balancing. **d**, **e** line balancing for two profiles (**a** and **b**). The extracted profiles are well line-balanced. *Colours* as in Fig. 3

sedimentary pile is too small, cross-sections have difficulties filling the space between the folded higher units and the floor thrust and often propose large offset thrusting of lower units (e.g. Laubscher 2008; Sommaruga 1997) or other poorly constrained shortening structures in the deep subsurface. The detachment fold model adopted

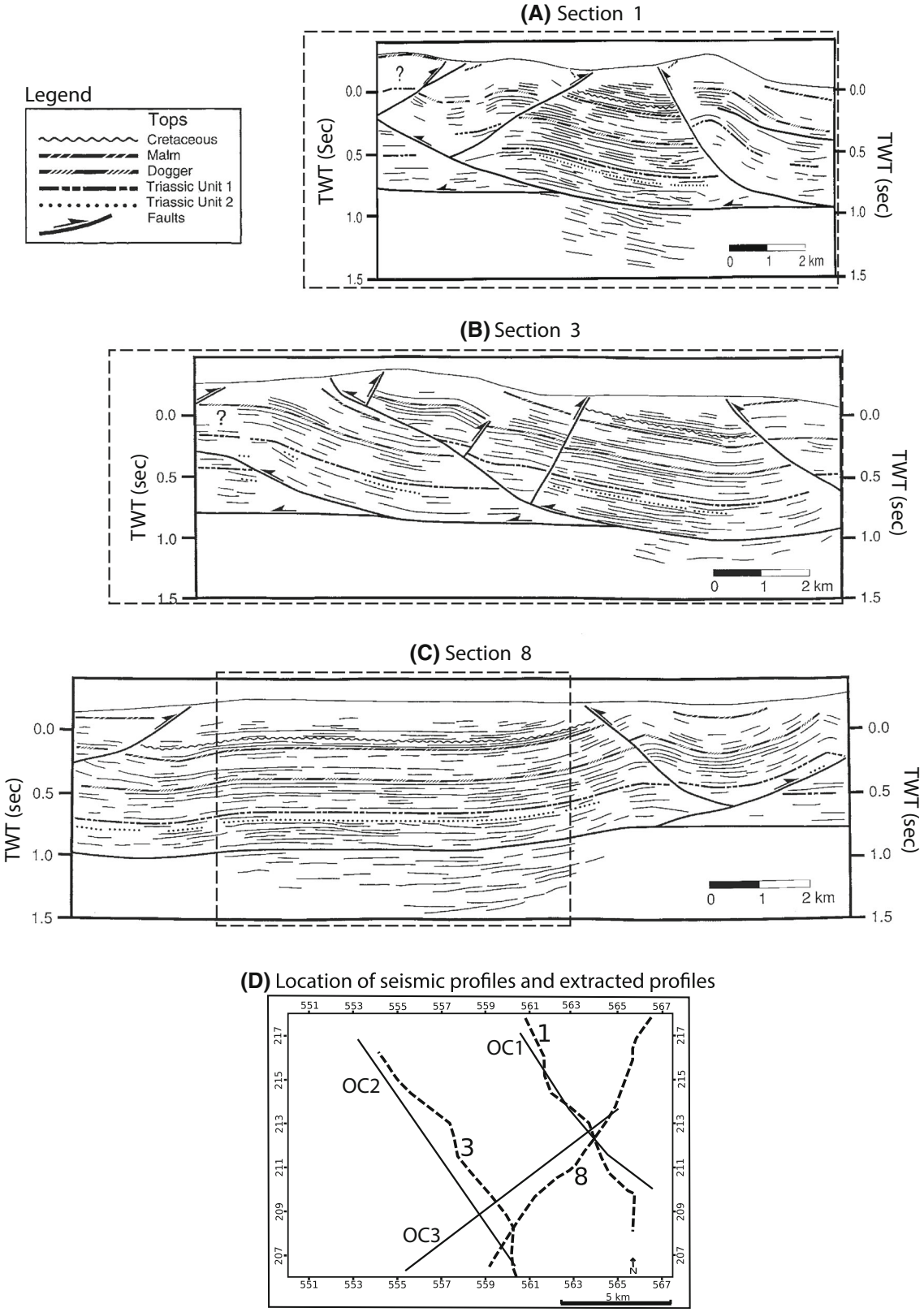

Fig. 8 a–c Seismic profiles along extracted cross-sections, from Sommaruga (1997). *Dashed* frames refer to the profiles as shown in Fig. 7. **d** Location of the seismic profiles (*dashed lines*) and extracted profiles (*solid lines*). Note close correspondence between seismic profiles and profiles extracted from the model

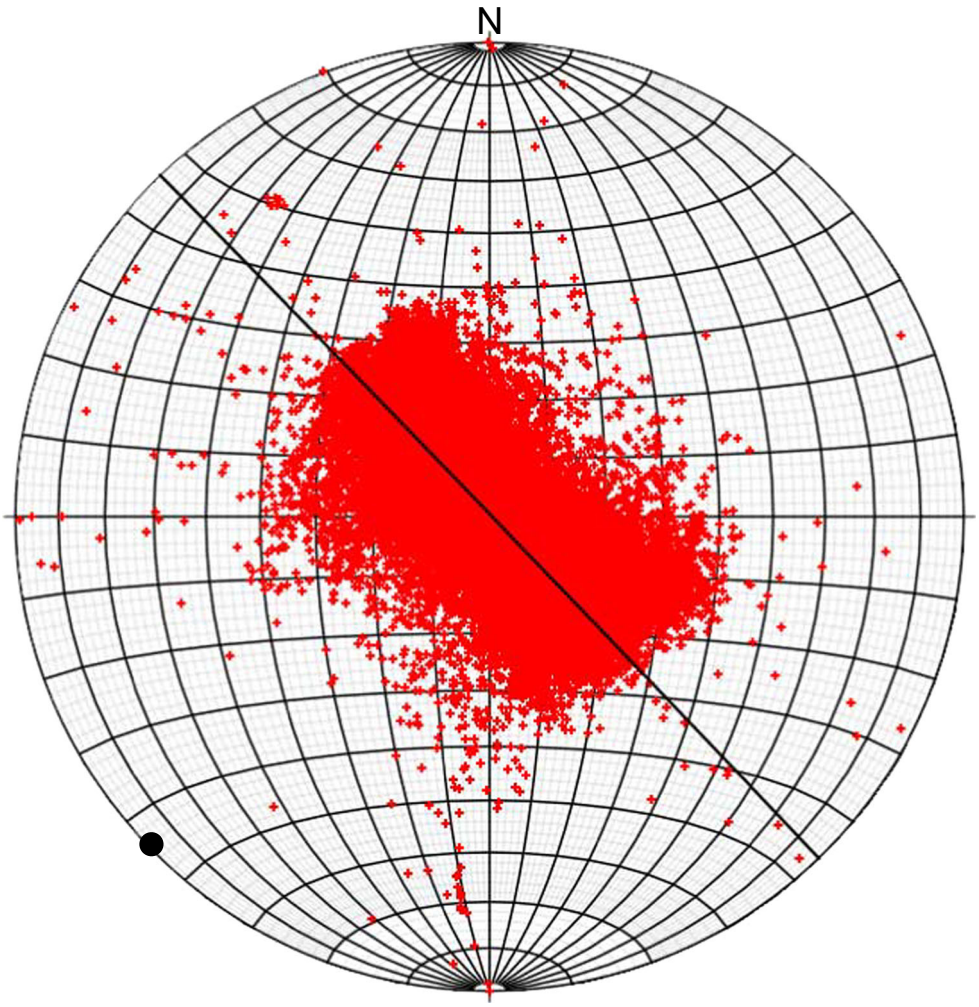

Fig. 9 Schmidt net (lower hemisphere) showing 82382 poles to the Earth's surface as calculated from the digital elevation model, for the entire model area. Best-fit *great circle* of the orientation distribution is indicated. *Filled circle* indicates calculated "topographic fold axis" oriented SW-NE, i.e. parallel to the average fold orientation in the area

here results in a larger average thickness of the Muschelkalk series and smaller associated amounts of shortening.

The 3D geometrical model was constructed using MOVE (version 2014) developed by Midland Valley Corporation. First the digital elevation model (DEM) and the geological map (1:250,000) of the area were implemented as a reference. In the next step, the key features of the area such as tear faults and thrust faults and also unit boundaries (called "horizons" in MOVE) on the surface were digitized according to the surface data and the geological map. Nine vertical cross-sections, which had been newly constructed and/or modified from Sommaruga (1997), were entered, and the structural architecture of each profile was digitised by using the Fault and Horizon tool. Finally, the synthetic three-dimensional model of the fold-and-thrust belt was constructed using the interpolation algorithm of MOVE between serial cross-sections. Thrust surfaces were constructed in the same way. For those surfaces (horizons, thrusts and faults) not defined between two adjacent cross sections (e.g. at the side of the model), the Extrusion Method of the software was used, which extrapolates lines based on the original specification in the desired trend or plunge direction.

The geometries of tear faults were designed in the following way. The two largest tear faults cut and offset the underlying ramp below the Tête de Ran anticline at shallow depth but root into them in the deeper parts of the section. Hence, the thrust is zipped by the tear faults down to a certain depth below which there is no offset (3D file in the supplementary material). In this way, the tear faults account for the offset of the thrust faults at the surface, but still preserve a continuous branch line with the major floor thrust. Minor tear faults were modelled as mere surfaces that produce no offset or only a small flexure in the horizons.

Figure 6 shows two views of the fault surfaces in three dimensions (for more surface and subsurface views of the model, we refer to the 3D file in the supplementary material). Once the 3D model (both surface and subsurface layers) has been completed, the software permits to examine it from various directions. In particular, it allows

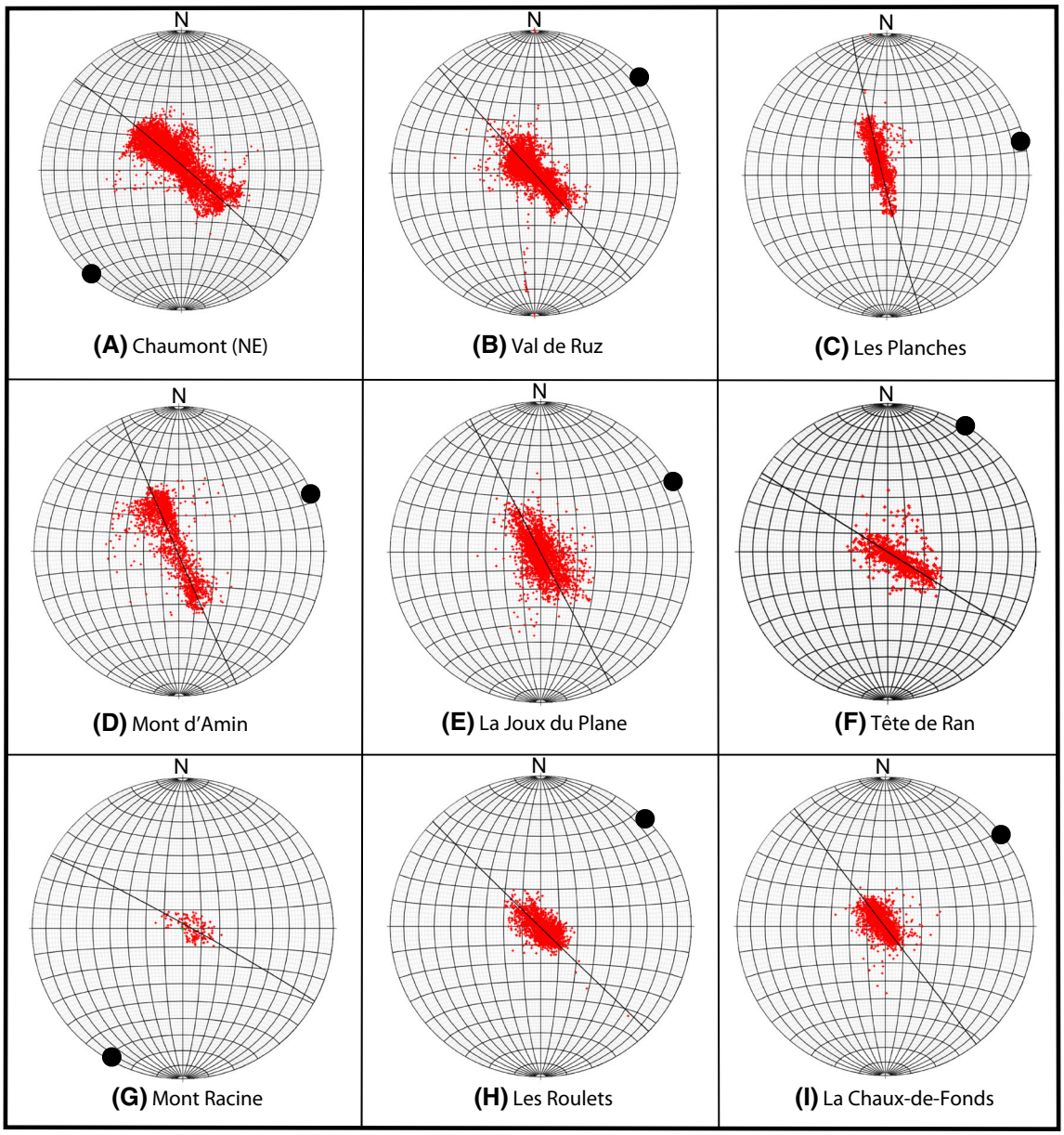

Fig. 10 Schmidt nets (lower hemisphere) showing orientation distribution of Earth's surface, determined from digital elevation model, for parts of the area. *Great circles* and *filled circles* as in Fig. 9. See Fig. 2 for location of the subareas, and Table 1 for comparison of the "topographic fold axes" with structural fold axes from Sommaruga and Burkhard (1997). The difference in trend is small for ENE-trending anticlines (e.g., Mont d'Amin) and partly large for NNE-trending anticlines (e.g., NE part of Chaumont)

the extraction of cross-sections in order to check the model against other available data and geological concepts. Corrections were made where the model showed inconsistencies, especially for tear-fault surfaces, where in some cases the interpolation algorithm resulted in dip angles contradicting the surface data.

3.2 Results and implications

Three cross-sections extracted from the 3D model, OC1, OC2, and OC3, are shown in Fig. 7 (for additional sections see electronic supplementary material). They are oriented approximately parallel to existing reflection seismic sections (Fig. 8). Two are perpendicular and one is parallel to the overall strike of fold axial planes. All three appear geologically plausible, except for very minor inconsistencies. Profile OC2 crosses the Tête de Ran anticline in the area where it is most strongly affected by the faults of the La Ferrière fault system. The thrust in the northwestern limb of this anticline is surprisingly steep in the profile; this may be a mistake in the model or, alternatively, result from interference with the strike-slip faults. One of the minor

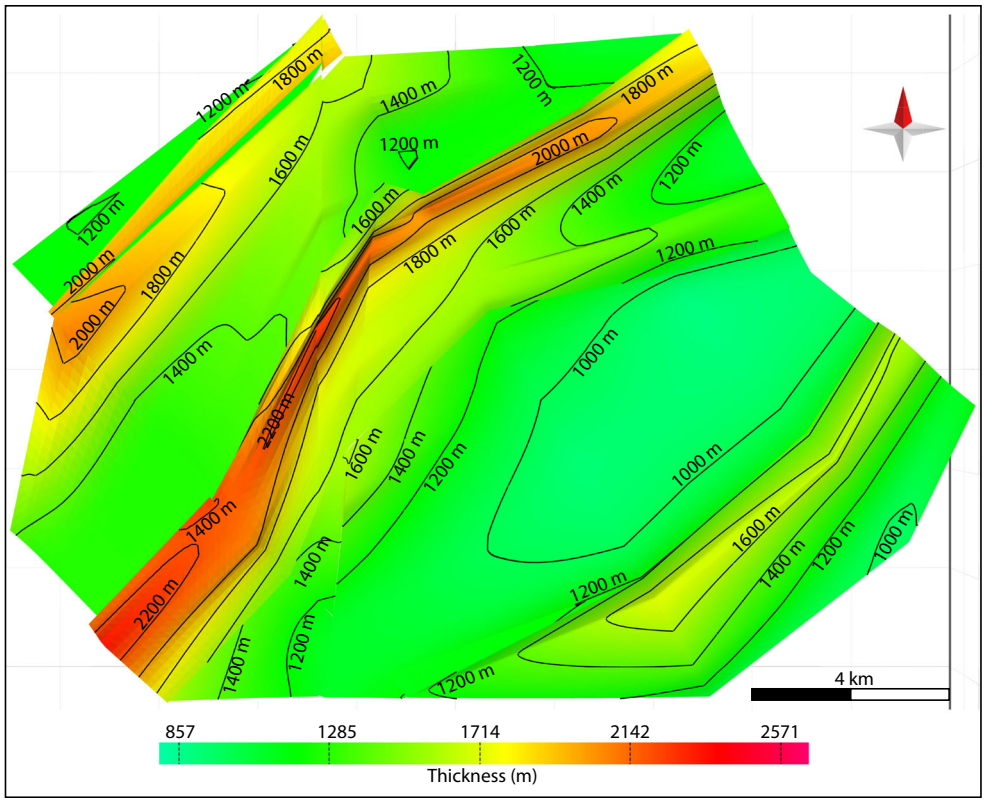

Fig. 11 "Tectonic" thickness of Muschelkalk, measured in a vertical direction from the top of the Muschelkalk down to the top of the basement, and shown in an oblique view. This *thickness* includes layer repetition by thrusting, leading to high thickness in anticlines. *Red* compass needle indicates north

faults of the La Ferrière system appears as a vertical fault in the core of the Tête anticline and roots in the thrust. It displays a small apparent offset, which is modelled as a flexure. All three cross-sections are consistent with seismic observations (Fig. 8), and the two sections perpendicular to the strike direction (Profile OC1 and OC2) are well-balanced (Fig. 7d, e).

The model also allows the extraction of statistical data on surface orientations including the topography and the illustration of this data in Schmidt nets, using the Vertex Attributes tools of MOVE. We applied this to the entire DEM of Val de Ruz and to specific anticlinal and synclinal areas in order to analyse the orientation of surfaces. Figures 9 and 10 show orientations of topography as lower-hemisphere poles to the DEM in the entire area and in local areas, respectively. Figure 9 for the entire area shows a broad girdle distribution. The dip directions of the steep slopes are predominantly northwest- and southeastward. The pole to the best-fit great circle of the orientation distribution defines a "topographic fold axis" in the same way as a fold axis is constructed for a girdle distribution of folded geological surfaces. This topographic fold axis is horizontal and trends SW (226°). Its orientation is similar to the average trend of fold axes in the area, showing that topography is strongly controlled by the folds. This reflects the fact that deformation in the Jura Mountains is rather young, most anticlines still coinciding with mountain ridges and synclines with valleys. The lithological succession with alternating limestone and marl layers leads to the top of limestone layers often forming the Earth's surface. The girdle in Fig. 9 is rather wide, which results partly from the variation in trend of the folds between north-northeast and east-northeast.

Some local-area Schmidt nets (Fig. 10c, f) display the asymmetry typical for fault-bend and fault-propagation anticlines: forelimbs of the folds and the associated topography are steeper than the back limbs and this structural asymmetry is reflected also in the topographic slope. The Schmidt net for the Chaumont anticline (Fig. 10a) shows a subordinate girdle representing west- and east-directed slopes, which are related to north–south-oriented strike-slip faults. Comparison of the topographic fold axes with "structural" fold axes determined from the analysis of bedding orientation measurements (Sommaruga and Burkhard, 1997; Tschanz and Sommaruga 1993) shows deviations of 21° and 11° for the Chaumont and the Tête de Ran anticlines, respectively (Tab. 1). In both areas, the topographic fold axis trends more northerly than the

Table 1 Comparison of "topographic fold axes" (plunge direction/dip angle) determined from orientation analysis of the digital elevation model with "structural fold axes" from Sommaruga and Burkhard (1997). Letters A to I refer to areas as indicated in Fig. 10

	A	B	C	D	E	F	G	H	I
Topographic fold axis data	221/04	047/01	076/03	247/01	062/01	212/01	209/04	045/02	052/02
Structural fold axis data	242/13	–	070/00	246/07	068/03	223/02	212/08	–	–

structural fold axis. Both anticlines are significantly influenced by north–south striking strike-slip faults. These anticlines can be imagined as arrays of small, more easterly-striking anticline fragments displaced by sinistral north–south strike-slip folds into an overall more northerly-striking alignment. This was also concluded by Sommaruga and Burkhard (1997) when they compared their structural fold axes with "map scale fold axis trends". To explain the wrenching of the NNE-trending anticlines, Sommaruga and Burkhard (1997) proposed that these anticlines were influenced by fault zones related to pre-Jura-folding, i.e. Oligocene normal faults that formed due to WNW-ESE-directed stretching of the Upper Rhine Graben system.

An example of thickness analysis derived from the final model is shown in Fig. 11 that shows the thickness of the Muschelkalk strata, measured in a vertical direction from the top to the base of the series. It shows values around 1000 m in the synclines and locally reaches more than 2000 m in the anticlines. We will discuss thickness variations in detail in the following.

4 Discussion

We briefly discuss a few aspects of the model: the implied thickness of the Muschelkalk strata, thickness variations within the Muschelkalk, and finally fault offset and deformation style.

The Muschelkalk strata have an average sedimentary thickness of around 1000 m according to our model (see detailed discussion below). Though relatively large, this thickness is perfectly reasonable in view of seismic and well data in- and outside the Jura Mountains and is also in line with other studies on the western Jura Mountains (Sommaruga 1997; Affolter and Gratier 2004). However, the top of the basement in the study area is not constrained by drilling and not imaged beyond doubt by reflection seismics. The Triassic formations might well be 200–300 m thinner if top basement would be shallower. The nearest well that penetrates the Triassic rocks, the above-mentioned well Treycovagnes-1 (Fig. 1), yielded more than a 1000 m of Triassic rocks. Most of these were actually imbricated Keuper sediments. Hence, it seems that at a regional scale the strata of the Keuper experience the same style of decoupled deformation as those of the Muschelkalk. In the Val de Ruz area, coherent deformation of Keuper and the overlying sequence is merely suggested by the regionally occurring reflector H (Sommaruga 1997).

It appears that thickness variations of the Triassic succession within and in the vicinity of the study occur at different scales and that they have different origins: (1) At the regional scale, the average thickness of Triassic strata continuously decreases by an order of magnitude from the Jura Mountains towards the Helvetic domain of the Alps and this variation is clearly of sedimentary origin (e.g. Sommaruga 1997). (2) Within the Jura Mountains, there are pronounced local thickness increases related to ramp-flat thrusting at the kilometre scale. (3) This thrusting appears to be superimposed on broader anti- and synclines at the scale of 5–10 km, which are related to lateral flow in the soft Triassic sediments and this deformation might at least partly be older than the thrusting. The wide Val de Ruz basin corresponds to a syncline of this sort. The average pre-deformation (pre-thrusting and pre-flowing) sedimentary thicknesses of the Muschelkalk strata along a cross section can be estimated by dividing the cross sectional area of the Muschelkalk between two pinlines by the original (retro-deformed) length of the now folded and thrusted sedimentary pile. Note that this length is well constrained by the length of the younger Mesozoic strata near the surface. Thicknesses of the Muschelkalk series derived by this approach are between 1010 and 1130 meters for four NW–SE-oriented cross sections (Fig. 4; D1: 1010 m, D2: 1025 m, D3: 1095 m, D8: 1130 m). This is 100–250 m thicker than the minimum thickness of the Muschelkalk below the Val-de-Ruz syncline. Hence, the thickness below the Val-de-Ruz syncline is significantly lower than the average pre-deformation sedimentary thickness and we interpret this deviation to be the result of horizontal flow from the syncline into the adjacent anticlines. The presence of salt leads to extremely weak detachment horizons and typically causes flow into anticlines during incipient deformation, as has been shown for several examples of fold-and-thrust belts, including the Jura Mountains (Davis and Engelder 1985).

Strictly law-abiding balancing assuming a constant thickness for the Triassic has led to far-reaching interpretations about the subsurface architecture such as local basement highs or complicated shortening geometries at

depth (e.g. Laubscher 2003) as the thickness has typically been inferred from the wide synclines where the original sedimentary thickness of the Triassic might be underestimated.

More than one thrust can nucleate from a flow-related larger-scale anticline leading to the occurrence of structurally high, narrow synclines in between. In order to explain a wide structural high, Schori et al. (2015) have proposed doubling of the older part of the stratigraphic succession along a detachment with several kilometres offset in the lower Middle Jurassic Opalinus clay for the map sheet "Chasseral" northeast of the study area. However, where the lower Middle Jurassic rocks reach the surface, e.g. on the next map sheet to the Northeast ("Moutier"), the Opalinus clay is coherently folded together with the older and younger Mesozoic successions and no detachment is present (Pfirter 1997). Also in tunnels the Opalinus clay has typically been found in stratigraphic succession (see Buxtorf 1916; Laubscher 2008; Caer et al. 2015). Large-wavelength folding at amplitudes of a few hundred meters accommodated by lateral flow in the Triassic is well documented by drilling and seismics in the Molasse Basin (Sommaruga 1997) but also in the more external Plateau Jura. The above-mentioned well Laveron-1 (Fig. 1) penetrates more than 1400 m of Triassic rocks, and reflection seismic data show a corresponding antiform with a wavelength of 10 kilometres below the reflector H (Sommaruga 1997). Such folding under the Internal Jura can explain structural highs more naturally than discrete fault-related structures. Our model also shows a gradual variation of structural level rather than discrete steps, which would be expected if highs and lows were controlled by faults. The observed upward bend of strata towards the anticlines even beneath the thrust ramps (Fig. 4, e.g. southern anticline in sections C1, C2, and C3) is in our view a further argument for lateral flow in the Triassic. Finally, thrust faults in the study area show at most a few hundred meters offset at the surface. In traditional balancing approaches, such thrusts often are displayed with kilometres of offset at depth since the rather wide backlimbs of antiforms are explained by the doubling of strata rather than by horizontal flow. Accordingly, our model predicts moderate shortening between 7 and 17%, which is less than typical reconstructions that assume an on the average thinner Triassic succession. The initial buckling stage may be associated with an unknown amount of distributed layer-parallel shortening and associated thickening (e.g. Frehner et al. 2012; Ghassemi et al. 2010). For this reason our shortening estimates are minimum values. We consider, however, distributed deformation to be limited since little or no internal deformation is found outside tectonized zones in the Jura (Tschanz 1990).

5 Conclusions

3D geometrical modelling resulted in a plausible subsurface model from which new kinematically balanced cross-sections can be extracted. The folds are decoupled from the basement in the evaporite-bearing Muschelkalk series. The Muschelkalk appears to show significant pre-thrusting thickness variations. This variation is at least partly due to lateral flow of the Triassic evaporites during the early phase of detachment folding, away from synclines and towards anticlines. Assuming a second decoupling horizon in the Dogger or involvement of the basement in the Jura tectonics is unnecessary for explaining the geology of the study area. Due to the young tectonics of the Jura Mountains, topography closely correlates with tectonic structure. Comparing "topographic" fold axes derived from orientation statistics of the Earth's surface with published "structural" fold axes confirms earlier suggestions that the trend of the NNE-trending folds was modified by small-scale NS-striking sinistral strike-slip faults similar to regional tear faults like the La Ferrière fault.

Acknowledgements We thank A. Sommaruga, M. Frehner, and editor S. Schmid for careful reviews that helped substantially to improve the paper.

References

Affolter, T., & Gratier, J.-P. (2004). Map view retrodeformation of an arcuate fold-and-thrust belt: The Jura case. *Journal of Geophysical Research, 109,* B03404. doi:10.1029/2002JB002270.

Aubert, D. (1945). Le Jura et la tectonique d'écoulement. *Mémoire de la Société Vaudoise des Sciences Naturelles, 8,* 217–236.

Bitterli, P. (1972). Erdölgeologische Forschungen im Jura. *Bulletin der Vereinigung Schweizerischer Petroleum-Geologen und –Ingenieure, 39*, 13–28.

Bourquin, P., Buxtorf, R., Frei, E., Lüthi, E., Mühlenthaler, C., Ryniker, K., et al. (1968). *Atlas géologique de la Suisse 1:25'000, feuille 51 Val de Ruz.* Basel: Commission géologique Suisse.

Bundesamt für Wasser und Geologie (2005). *Geologische Karte der Schweiz 1:500 000.* Bern-Ittingen.

Burkhard, M. (1990). Aspects of the large-scale Miocene deformation in the most external part of the Swiss Alps (Subalpine Molasse to Jura fold belt). *Eclogae Geologicae Helvetiae, 83,* 559–583.

Buxtorf, A. (1907). *Geologische Beschreibung des Weissensteintunnels und seiner Umgebung*. Beiträge zur Geologischen Karte der Schweiz (N.F.), 21.

Buxtorf, A. (1916). Prognosen und Befunde beim Hauensteinbasis- und Grenchenbergtunnel und die Bedeutung der letzteren für die Geologie des Juragebirges. *Verhandlungen der Naturforschenden Gesellschaft in Basel, 27,* 184–254.

Caer, T., Maillot, B., Souloumiac, P., Leturmy, P., Frizon de Lamotte, D., & Nussbaum, F. (2015). Mechanical validation of balanced cross-sections: The case of the Mont Terri anticline at the Jura front (NW Switzerland). *Journal of Structural Geology, 75,* 32–48.

Davis, D. M., & Engelder, T. (1985). The Role of Salt in Fold-and-Thrust Belts. *Tectonophysics, 119,* 67–88.

Diebold, P. (1988). Der Nordschweizer Permokarbon-Trog und die Steinkohlenfrage der Nordschweiz. *Vierteljahrsschrift der Naturforschenden Gesellschaft in Zürich, 133,* 143–174.

Fischer, H. & Luterbacher, H. (1963). *Das Mesozoikum der Bohrungen Courtion 1 (Kt. Fribourg) und Altishofen 1 (Kt. Luzern).* Beiträge zur Geologischen Karte der Schweiz (N.F.), 115, 40 pp.

Frehner M., Reif D. & Grasemann B. (2012): Mechanical versus kinematical shortening reconstructions of the Zagros High Folded Zone (Kurdistan Region of Iraq). *Tectonics 31*, TC3002, doi:10.1029/2011TC003010.

Ghassemi, M. R., Schmalholz, S. M., & Ghassemi, A. R. (2010). Kinematics of constant arc length folding for different fold shapes. *Journal of Structural Geology, 32,* 755–765. doi:10.1016/j.jsg.2010.05.002.

Gorin, G. E., Signer, C., & Amberger, G. (1993). Structural configuration of the western Swiss Molasse Basin as defined by reflection seismic data. *Eclogae Geologicae Helvetiae, 86,* 693–716.

Grasemann, B., & Schmalholz, S. M. (2012). Lateral fold growth and fold linkage. *Geology, 40,* 1039–1042. doi:10.1130/G33613.1.

Groupe de travail PGN (2008). *Evaluation du potentiel géothermique du canton de Neuchâtel (PGN).* Vol.1: Rapport final, Vol.2: Annexes, CREGE 11-08/02, Neuchâtel; http://www.ne.ch/autorites/DDTE/SCAT/Documents/02_Plan_directeur_cantonal/Evaluation_potentiel_geothermique_canton_Neuchatel.pdf.

Guellec, S., Mugnier, J. L., Tardy, M. & Roure, F. (1990). Neogene evolution of the western Alpine foreland in the light of ECORS data and balanced cross sections. In: Roure, F., Heitzmann, P. & Polino, R. (Eds.), Deep structure of the Alps. *Mémoire de la Société Géologique Suisse*, *1*, 165–184.

Jordan, P. (1992). Evidence for large scale decoupling in the Triassic evaporites of Northern Switzerland: an overview. *Eclogae Geologicae Helvetiae, 85,* 677–693.

Kälin, D. (1997). Litho- und Biostratigraphie der mittel- bis obermiozänen Bois de Raube – Formation (Nordwestschweiz). *Eclogae Geologicae Helvetiae, 90,* 97–114.

Keller, W.T. & Liniger, H. (1930). *Geologischer Atlas der Schweiz, Blätter 92-95 Movelier–Soyhieres–Delemont–Courrendlin*. Schweizerische Geologische Kommission.

Laubscher, H. P. (1961). Die Fernschubhypothese der Jurafaltung. *Eclogae Geologicae Helvetiae, 54,* 221–280.

Laubscher, H. P. (1965). Ein kinematisches Modell der Jurafaltung. *Eclogae Geologicae Helvetiae, 58,* 231–318.

Laubscher, H. P. (1972). Some overall aspects of Jura dynamics. *American Journal of Science, 272,* 293–304.

Laubscher, H. P. (2003). Balanced sections and the propagation of décollement: A Jura perspective. *Tectonics, 22*, article 1063, doi:10.1029/2002TC001427.

Laubscher, H. (2008). The Grenchenberg conundrum in the Swiss Jura: a case for the centenary of the thin-skin décollement nappe model (Buxtorf 1907). *Swiss Journal of Geosciences*, *101*(1), 41–60. doi:10.1007/s00015-008-1248-2.

Loup, B. (1992). Mesozoic subsidence and stretching models of the lithosphere in Switzerland (Jura, Swiss Plateau and Helvetic realm). *Eclogae Geologicae Helvetiae, 85,* 541–572.

Madritsch, H., Fabbri, O., Hagedorn, E.-M., Preusser, F., Schmid, S. M., & Ziegler, P. A. (2010). Feedback between erosion and active deformation: geomorphic constraints from the frontal Jura fold-and-thrust belt (eastern France). *International Journal of Earth Sciences, 99*(Suppl. 1), S103–S122.

Madritsch, H., Schmid, S.M. & Fabbri, O. (2008). Interactions between thin- and thick-skinned tectonics at the northwestern front of the Jura fold-and-thrust belt (eastern France). *Tectonics, 27*, TC5005, doi:10.1029/2008TC002282.

Malz, A., Madritsch, H., Meier, B., & Kley, J. (2016). An unusual triangle zone in the external northern Alpine foreland (Switzerland): Structural inheritance, kinematics and implications for the development of the adjacent Jura fold-and-thrust belt. *Tectonophysics, 670,* 127–143.

Marquer, D., Calcagno, P., Barfety, J.-C., & Baudin, T. (2006). 3D modeling and kinematics of the external zone of the French Western Alps (Belledonne and Grand Chatelard Massifs, Maurienne Valley, Savoie). *Eclogae Geologicae Helvetiae, 99,* 211–222.

Maxelon, M., & Mancktelow, N. S. (2005). Three-dimensional geometry and tectonostratigraphy of the Pennine zone, Central Alps, Switzerland and Northern Italy. *Earth Science Reviews, 71,* 171–227.

Mitra, S. (2003). A unified kinematic model for the evolution of detachment folds. *Journal of Structural Geology, 25,* 1659–1673.

Pavoni, N. (1961). Faltung durch Horizontalverschiebung. *Eclogae Geologicae Helvetiae, 54,* 515–534.

Pfiffner, O. A., Erard, P.-F. & Stäuble, M. (1997). Two cross sections through the Swiss Molasse Basin (lines E4-E6, W1, W7-W10). In: Pfiffner, O. A. et al. (Eds.): *Deep structure of the Swiss Alps, results of NFP 20.* Birkhäuser Verlag Basel, 73–100.

Pfirter, U. (1997). *Atlas géologique de la Suisse 1:25,000, feuille 1106 Moutier*. Basel: Commission géologique Suisse.

Philippe, Y., Colletta, B., Deville, E., Mascle, A. (1996). The Jura fold-and-thrust belt: a kinematic model based on map-balancing. In: Ziegler, P.A. & Horvath, F. (Eds.): *Peri-Tethys Memoir 2: Structure and prospects of Alpine basins and forelands*. Mémoires du Muséum National d'Histoire Naturelle, Paris, 170, 235-261.

Sala, P., Pfiffner, A. O., & Frehner, M. (2014). The Alpstein in three dimensions: fold-and-thrust belt visualization in the Helvetic zone, eastern Switzerland. *Swiss Journal of Geosciences, 107,* 177–195.

Schori, M., Mosar, M., & Schreurs, G. (2015). Multiple detachments during thin-skinned deformation of the Swiss Central Jura: a kinematic model across the Chasseral. *Swiss Journal of Geosciences, 108,* 327–343.

Sommaruga, A. (1995). Tectonics of the central Jura and the Molasse Basin. New insights from the interpretation of seismic reflection data. *Bulletin de la Société Neuchatêloise des Sciences Naturelles, 118,* 95–108.

Sommaruga, A. (1997). Geology of the Central Jura and the Molasse Basin: New insight into an evaporite-based foreland fold and thrust belt. *Mémoire de la Société Neuchatêloise des Sciences Naturelles, 12,* 1–176.

Sommaruga, A. (1999). Décollement tectonics in the Jura foreland fold-and-thrust belt. *Marine and Petroleum Geology, 16,* 111–134.

Sommaruga, A. & Burkhard, M. (1997). Interpretation of seismic lines across the rhomb shaped Val-de-Ruz Basin (internal Folded Jura). In: Pfiffner, O.-A. et al. (Eds.), *Deep structure of the Swiss Alps, results of NFP 20.* BirkhäuserVerlag Basel, 45–53.

Sommaruga, A., Eichenberger, U. & Marillier, F. (2012). *Seismic Atlas of the Swiss Molasse Basin*. Beiträge zur Geologie der Schweiz—Geophysik, 44.

Suppe, J. (1983). Geometry and kinematics of fault-bend folding. *American Journal of Science, 283,* 684–721.

Suppe, J., & Medwedeff, D. A. (1990). Geometry and kinematics of fault-propagation folding. *Eclogae Geologicae Helvetiae, 83,* 409–454.

Tanner, D., Behrmann, J., & Dresmann, H. (2003). Three-dimensional retro-deformation of the Lechtal nappe, Northern Calcareous Alps. *Journal of Structural Geology, 25,* 737–748.

Tschanz, X. (1990). Analyse de la déformation du Jura central entre Neuchâtel (Suisse) et Besançon (France). *Eclogae Geologicae Helvetiae, 83,* 543–558.

Tschanz, X., & Sommaruga, A. (1993). Deformation associated with folding above frontal and oblique ramps around the rhomb shaped Val de Ruz basin. *Annales Tectonicae, 7,* 53–70.

Ustaszewski, K. & Schmid, S.M. (2006). Control of preexisting faults on geometry and kinematics in the northernmost part of the Jura fold-and-thrust belt. *Tectonics, 25*, TC5003, doi: 10.1029/2005TC001915.

Zanchi, A., Salvi, F., Zanchetta, S., Sterlacchini, S., & Guerra, G. (2009). 3D reconstruction of complex geological bodies: examples from the Alps. *Computers & Geosciences, 35,* 49–69.

Ziegler, P. A. (1982). *Geological Atlas of Western and Central Europe* (p. 130). Den Haag: Shell Internationale Petroleum Maatschappij B.V.